npj | vaccines

Article

Published in partnership with the Sealy Institute for Vaccine Sciences

https://doi.org/10.1038/s41541-025-01199-6

Optimized lentiviral backbone induces robust and diverse T cell immunity against neoantigens to counteract tumor heterogeneity

Benjamin Vesin[1], Ingrid Fert[1], Amandine Noirat[1], Pierre Authié[1], Sylvain Ciret[1], Catherine Blanc[1], Yakov Vitrenko[2], Pierre Charneau[1], Laleh Majlessi[1] & François Anna[1] ✉

Targeting personalized tumor neoantigens is a promising strategy in immuno-oncotherapy, tumor heterogeneity requires that adaptive immunity be effectively induced against a broad spectrum of neoantigens for a significant anti-tumor effect. We developed several non-integrative lentiviral vectors encoding optimized immunogen that induce robust T cell responses against neoepitopes derived from murine colorectal tumors. Incorporating proteasome-targeting sequences and 4-alanine spacers between neoepitopes enhanced responses to both dominant and subdominant neoepitopes. Using longer natural sequences encompassing minimal epitopes further improved immunogenicity. These vectors drove complete regression of MC38 tumors expressing the selected neoepitopes and sustained immune memory to prevent relapse. Additionally, these vectors synergized with anti-programmed cell death protein 1 (PD1) therapy to inhibit wild-type MC38 tumor growth. Variant allele frequency tracking demonstrated T cells eradicated neoantigen-positive cells without affecting negative ones. Our results validate lentiviral vectors for personalized neoepitope therapy and underscore the need for diverse neoantigens in immunotherapy against tumor mosaicism.

Targeting neoepitopes specifically generated by neo-mutations exclusive to a patient's tumor represents a promising immuno-oncotherapy strategy. Advances in high-throughput gene sequencing, genomic or transcriptional profiling and improved epitope prediction tools, have enabled this strategy to move from an academic perspective to medical applications[1]. The principal indications for neoantigen-based immuno-oncotherapy are melanoma, non-small cell lung and colorectal cancers, characterized by high mutation burdens[2]. The unceasing intra-tumoral emergence of neo-mutations generates a tumor genetic mosaicism. Therefore, to maximize the coverage of the tumor heterogeneity, the immunotherapy has to include a diversified neoepitope repertoire, representative of this mutational diversity in sufficient proportions of tumor cells and in various sectors of the primary and metastatic tumors[3,4].

Generation of DNA-, mRNA- or viral vector-based vaccines, encoding assortment of multiple neoepitopes, requires concatenation of the gene segments which gives rise to a chimeric protein of unknown structure, stability and degradability by proteases. Given the time constraints associated with personalized immuno-therapeutic strategies, including neoantigen identification, vaccine design and GMP production[5], the availability of an effective vaccine platform with an optimal universal backbone able to carry the selected epitopes is essential. The chosen vaccine platform must be capable of inducing significant $CD4^+$ or $CD8^+$ T cell responses against epitopes of non-verified affinity for Major Histocompatibility Complex (MHC) molecules. Therefore, not only a powerful and safe immunization vector is necessary, but also the antigen design must have the potential to facilitate processing and presentation of each neoepitope without compromising the presentation of the other epitopes.

In this study, we evaluated the potential of non-integrative lentiviral vectors (LVs) to induce T cell responses against multiple personal neoantigens that we designed and optimized for their access to antigen presentation pathways. LVs are highly effective in eliciting strong and durable T-cell responses, even at low doses and with minimal inflammatory effects[6,7]. This efficiency is largely due to their ability to directly deliver transgenic antigens to dendritic cells (DCs), leading to endogenous antigen production within these cells. The safety of LVs is based on their non-replicative, non-cytopathic, and self-inactivating properties[8,9]. In

[1]Virology Department, Pasteur-TheraVectys Joint Lab, Institut Pasteur, Université Paris Cité, Paris, France. [2]Biomics Technology Plateform, Institut Pasteur, Université Paris Cité, Paris, France. ✉e-mail: francois.anna@pasteur.fr

non-integrative forms, mutations in the integrase enzyme prevent the integration of viral DNA into the host genome, resulting in persistence of episomal form of the transgenic DNA in the host cell nucleus. These episomes are gradually lost through cell division or death. The safety profile of LVs has been demonstrated in phase I clinical trials[10,11].Based on neoantigens previously described in MC38 (H-2^b) or CT26 (H-2^d) murine colon carcinoma models[12–14], we demonstrated that fusion of a poly-neoepitope to the proteasome targeting protein ubiquitin C, together with insertion of a hydrophobic 4-alanine spacer between consecutive short neoepitopes, strongly enhanced induction of T cell responses against both dominant and sub-dominant neoepitopes. The LVs encoding neoantigen designs that most broadened the diversity of T cell responses were the most effective in immunotherapy of MC38 or CT26 tumors. Our results also demonstrated that the use of 27-mers encompassing neoepitopes, compared to minimal 8- to 10-mer sequences, favored immunogenicity. The use of 27-mers also simplifies the approach as dispenses with the need for very precise neoepitope mapping.

A single injection of an LV-based vaccine fully eradicated an MC38 tumor engineered to homogeneously express an assortment of the targeted neoantigens. The same treatment also resulted in a significant delay in the growth of wild type (WT) MC38 tumors, which was improvable by combination with programmed cell death-1 (PD1) checkpoint blockade. These observations reinforced that the tumor genetic mosaicism poses a significant challenge in neoantigen-based immuno-oncotherapy. NGS analysis of Variant Allele Frequency (VAF) in the residual WT MC38 tumors from LV-treated mice revealed a decrease of the percentage of cells carrying neomutations suggesting efficient eradication by our vaccines. Tumor persistence seems to rely on wild-type cells that escaped the vaccine-induced T cell immunity. The signature of neoepitope-specific T cells correlated with the clearance of tumor subpopulations carrying alleles encoding the selected neoantigens. Altogether, these observations validate the proof-of-concept of the use of lentiviral vectors encoding personal neoepitopes in optimized designs for immuno-oncotherapy and also reinforce the need to include diversified tumor neoepitopes in immunotherapy immunization vectors to face tumor genetic mosaicism.

Results

Optimized design of poly-neoantigen backbone

Like any genetic vaccine, LV relies on the intracellular antigen presentation machinery for production, degradation and presentation of encoded immunogens through the MHC-I pathway. To optimize the degradation step, two strategies were implemented: (i) tagging the antigenic polypeptides with sequences that target them to proteasome, and (ii) insertion of spacers between consecutive peptide sequences to improve cleavage of each individual epitope while preventing interference with the processing of the others. For proteasome targeting, a murine ubiquitin C monomer, harboring the G76V mutation which prevents the ubiquitin C autocleavage was fused to the N-terminus[15]. The fusion with ubiquitin C tag mimics the initiation of ubiquitination pathway[16], facilitating proteasomal protein recognition and degradation, which enhances epitope availability for MHC-I presentation and therefore improves T-cell immunogenicity. This approach has been successfully used to generate T cell responses against subdominant epitopes of human papilloma virus (HPV), murine cytomegalovirus (mCMV) or influenza viruses[17–19]. Alternatively, a murine PEST sequence, rich in proline (P), glutamic acid (E), serine (S) and threonine (T), from ornithine decarboxylase was added to the C-terminus of the antigenic polypeptide[20]. The PEST sequence is a destabilizing sequence that can act as anchor site of E3 ubiquitin ligases, ensuring efficient turnover and antigen processing[21,22]. By reducing the half-life of generated chimeric proteins with unknown functions, these sequences can also minimize their potential toxicity. Since both ubiquitin C and PEST sequences are of murine origin, they are not expected to elicit an immune response in mice.

In addition, as part of the design optimization process, three distinct 4-mer spacers were inserted between consecutive epitopes: (i) 4-glycine spacer which provides apolar spacing, (ii) 4-alanine spacer which, through their hydrophobic nature promotes proteasome-mediated cleavage and ERAP 1-2 (endoplasmic reticulum aminopeptidases 1-2) trimming[23,24], or (iii) a Ser-Leu-Val-Arg (SLVR) sequence which enhances cleavage by lysosomal cathepsin, supporting epitope cross-presentation[25].

Seven CD8$^+$ T cell neoepitopes, i.e, Aatf, Adpgk, Cpne1, Dpagt1, Irgq, Med12 and Reps1, previously described in the MC38 murine colorectal cell line[12], were used to comparatively evaluate the potential of these antigen optimizations in an experimental LV-based immuno-oncotherapy. Distinct constructs were introduced into non-integrative LVs under the transcriptional control of human β2-microglobulin promoter for strong expression in antigen-presenting cells[6] and a post-transcriptional regulatory element (Wm) to enhance mRNA stability and nuclear export[23] (Fig. 1a).

Down selection of the most efficient proteasome-addressing tag and neoepitope spacer

We comparatively assessed the T cell immunogenicity of individual LVs encoding each of the optimized backbones and carrying the set of 7 selected MC38-derived neoantigens (Fig. 1b).

C57BL/6 J mice were intramuscularly (i.m.) vaccinated with 1×10^9 transduction units (TU) of LV-based vaccines or a transgene-free LV ("Ctrl LV") (Fig. 2a). Fourteen days post-injection, an IFNγ ELISPOT was applied to splenocytes, stimulated with synthetic peptides carrying individual neoepitope or the corresponding WT sequence (Fig. 2b, c).

Cpne1, Reps1, Adpgk, and Med12 neoepitopes, inducing >1000 spot-forming units (SFU) per 10^6 splenocytes, were defined as dominant, while Irgq, Aatf, and Dpagt1 neoepitopes, inducing <1000 SFU per 10^6 splenocytes, were defined as sub-dominant (Fig. 2b). Only Irgq, Cpne1 and Adpgk induced T cells able to discriminate the mutated and WT sequences. Notably, Med12 elicited a stronger T cell response against the WT versus the mutated sequence.

Cumulative SFU against the 7 neoepitopes enabled a better visualization of the intensity of the overall response (Fig. 2c–f). Among the LVs encoding constructs carrying various spacers, only LV::A7, carrying a 4-alanine spacer gave rise to a significantly increased cumulative response compared to LV::conca which had no spacer (Fig. 2c).

The addition of a proteasome-addressing tag, either ubiquitin C or PEST, significantly increased the response only when SLVR (Fig. 2d), but not the 4-alanine spacers, were used (Fig. 2e). The constructs carrying a proteasome addressing sequence, in association with a 4-alanine or SLVR spacer, showed no significant difference in overall response intensity (Fig. 2f). Both strategies aim to enhance epitope generation and may ultimately converge in their effect on overall immunogenicity. The presence of hydrophobic regions alone appears sufficient to promote efficient cleavage, thereby supporting robust T cell responses. However, in situations where these hydrophobic regions are not optimized, proteasome targeting may serve as a compensatory mechanism to maintain or enhance immunogenic potential.

Given that each neoantigen is potentially expressed by only a fraction of the overall tumor population, in addition to the intensity of the T cell responses, a relatively equal T cell response against all included neoepitopes may also be decisive in the antitumor efficacy. Figure 2g shows the distribution of median response between the neoepitopes for each construct. Although the overall response intensity was similar, the distribution of neoepitope T-cell specificities varied qualitatively among the various constructs. For instance, LV::conca favored induction of T cells against the dominant Cpne1 neoepitope, whereas all other LVs spacer-containing constructions, except LV::G7, produced consistent responses against the dominant Med12 neoepitope and the subdominant Irgq neoepitope. Only LV::UBA7 and LV::A7PEST elicited immune responses against the sub dominant Dpagt1 and Aatf epitopes in most of mice. Of note, these constructs carry either ubiquitin C or PEST proteasome-addressing sequence, and the 4-alanine spacers. These results illustrated that the use of spacers, particularly 4-alanine, together with a proteasome-addressing sequence, favored neoepitope presentation on MHC-I molecules antigen leading to the induction of intense and diversified T cell responses.

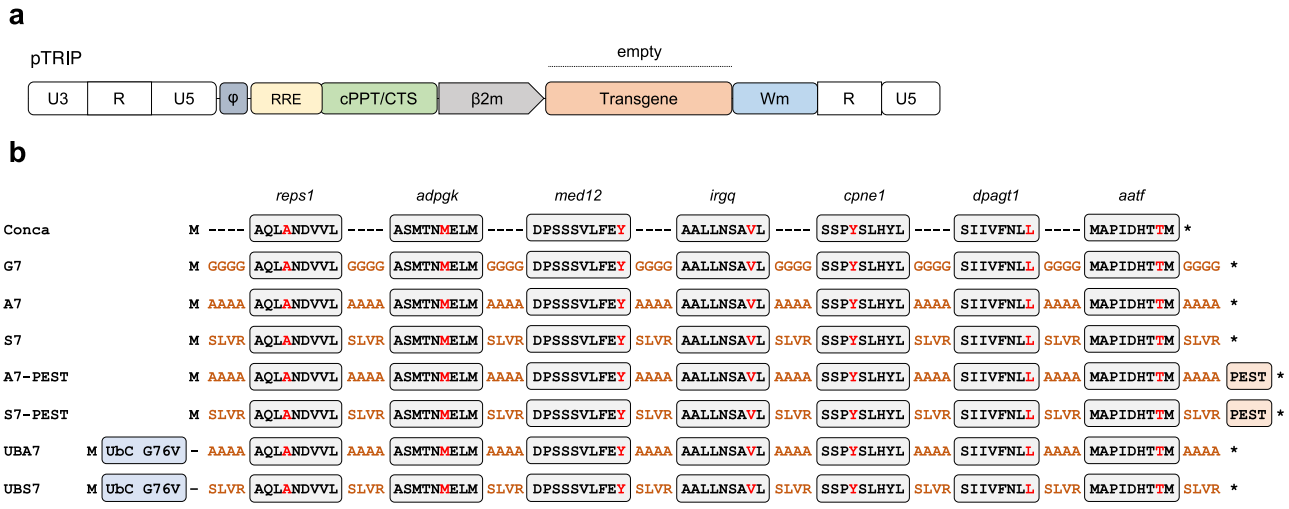

Fig. 1 | Design of LVs optimized for poly-neoepitope presentation. a Schematic representation of the transcriptional unit used for LV vector RNA production: U3RU5: 5' Long Terminal Repeat; φ: encapsidation signal; RRE: Rev Response Element; cPPT/CTS: central PolyPurine Tract / Central Termination Sequence; β2m: Beta-2-microglobulin promoter; Wm: Woodchuck Post-transcriptional Regulatory Element with the internal HBx protein ORF mutation, M1A. **b** Schematic representation of optimization neoepitope design to enhance presentation through the MHC-I endogenous pathway. Selected $CD8^+$ MC38-specific neoepitope sequences are shown in gray boxes, with mutated residues highlighted in red, spacer sequences in brown and proteasome addressing sequences in blue/red boxes. UbC G76V: Mouse ubiquitin C with a mutation of cleavage site G76V (Uniprot: P0CG50 - aa 1-76). PEST: PEST sequence from mouse Ornithine Decarboxylase (Uniprot: P00860 - aa 422-461).

For subsequent experiments, we selected constructs containing the 4-alanine spacer, since this modification significantly enhanced the immunogenicity. Among these constructs, LV::A7 was chosen based on its overall superior immunogenicity. We also included a comparable construct, i.e., LV::UBA7, which carries both the 4-alanine spacer and a proteasome-targeting sequence, as it elicited a broader immune response, particularly against subdominant Dpagt1 and Aatf epitopes. LV::UBA7 was preferred over LV::A7PEST because it is potentially easier to translate to humans. In fact, human and mouse Ubiquitin-C sequences are identical, whereas the ornithine decarboxylase-derived PEST, shows only 75% sequence homology between the species. Since the constitutive proteasome and immunoproteasome are structurally and functionally highly similar between the two species, the advantage of employing hydrophobic spacers is expected to be conserved in human[24].

Strong anti-tumor efficacy of LV::A7 and LV::UBA7 against an MC38 tumor homogeneously expressing the targeted neoantigens

Various MC38 cell lines used in different laboratories do not share a homogeneous neoepitope profile[26]. To assess the anti-tumor efficacy of T cell responses induced by LV::A7 and LV::UBA7, we first engineered an MC38 clone which stably and uniformly expresses a fusion of the 7 selected neoepitopes ("MC38 NeoAg") (Fig. 3a and Supplementary Fig. 1). Even though this model mitigates the neoantigen repertoire variability compared to the parental MC38 line, it provides a reliable platform to evaluate the immuno-therapeutic potential of the developed vectors. The MC38 NeoAg expression levels of H2-K^b, H2-D^b and PD-L1 were identical to those of the parental MC38 WT line (Fig. 3b), ensuring that potential differences in the T-cell induced tumor regression could be attributed to the neoantigen expression profile rather than to variations in these key immune-related proteins.

C57BL6/J mice were engrafted subcutaneously (s.c.) with 2.5×10^5 MC38::NeoAg cells. At day 6, when the tumors were palpable, mice received i.m. 1×10^9 TU of LV::conca, LV::G7, LV::A7, LV::UBA7 or Ctrl LV (Fig. 3c). All our LV constructs induced at least partial tumor regression from day 20 on. Some mice experienced tumor relapse by day 30, with the proportion of relapse varying among the tested vectors. Six of 7 mice treated with LV::conca or LV::G7 exhibited only partial tumor regression, followed by relapse. This profile was defined as partial response. In contrast, tumor eradication, defined as total response, was observed in 4 of 7 LV::A7-treated mice and in 3 of 7 LV::UBA7-treated mice. The remaining mice showed partial responses (Fig. 3d). By day 55, survival rates were significantly higher in the groups of LV::A7 and LV::UBA7 compared to the other groups (Fig. 3e). LV::A7 and LV::UBA7 demonstrated similar efficacy, as evidenced by the proportion of mice achieving complete responses (Fig. 3f) and by the average area under curve (AUC) of tumor growth on day 55 (Fig. 3g).

To evaluate the prospective immune memory, mice with complete regression were rechallenged on day 55 by s.c. implantation of 2.5×10^5 MC38 WT cells (Fig. 3h). The tumor growth was completely prevented in all mice originally treated with LV::UBA7, whereas 3 of 4 mice originally treated with LV::A7 developed tumors after the rechallenge. The 3 mice in the LV::A7 group that developed tumors showed no delay in tumor growth compared to untreated mice, suggesting an ineffective memory response. These results supposed a difference in the quality of the immune responses induced in mice treated with LV::UBA7 rather than LV::A7, which may be linked to with the superior potential of LV::UBA7 at eliciting T cells against subdominant epitopes (Fig. 2).

The MC38 Ag tumor model expresses all targeted neoantigens homogeneously, making it uniformly susceptible to immune responses directed against any one of them. Among the various vaccine designs, LV::A7 and LV::UBA7 elicited the most robust cumulative immune responses compared to LV::conca and LV::G7 (Fig. 2), and consequently had a greater impact on tumor growth in this model. However, when reintroducing the WT MC38 tumor, a broader and more diverse immune repertoire was required to address the full extent of its intrinsic heterogeneity. The limited immunogenicity of the LV::A7 vaccine toward specific neoepitopes such as Aatf and Dpagt1 (Fig. 2g) could allow tumor cells which express only these antigens to evade immune surveillance upon rechallenge. In contrast, the LV::UBA7 vaccine appears to overcome this limitation by effectively targeting these epitopes.

Partial inhibition of MC38 WT tumor growth and its relationship with vaccine-induced T cell diversity and intensity

We then addressed the effects of LV::A7 or LV::UBA7 treatment on the MC38 WT growth and tumor-infiltrating T cells (TILs). MC38 WT cells (2.5×10^5) were transplanted s.c. into C57BL/6 J mice and when the tumor

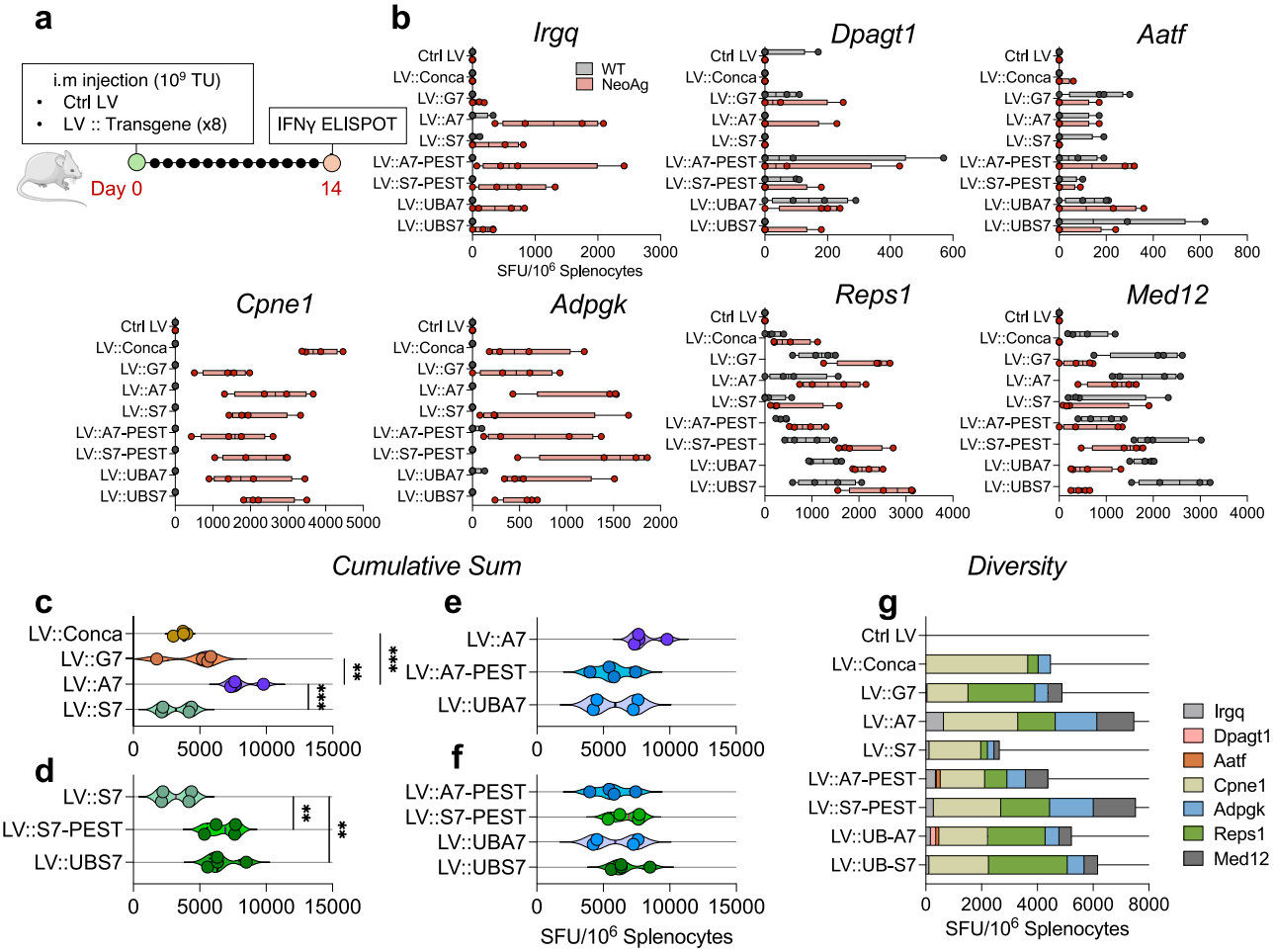

Fig. 2 | Optimized neoepitope designs favored specific T-cell immunogenicity. **a** Experiment timeline. **b** Evaluation of neoepitope-specific T cell responses by IFNγ ELISPOT ($n = 4$). **b**. SFU per LV design detected against WT (gray whiskers boxes) or mutated peptides (red whiskers boxes). Cumulative sum of all SFU/10^6 splenocytes for the 7 mutated peptides in individual mice, cross compared according to their spacers (**c**), association of each spacer with a proteasome-targeting sequence (**d**, **e**), or the combination of the latter (**f**). Statistical significance was determined by one-way ANOVA (** = $p < 0.01$; *** = $p < 0.001$). **g** Stacked bar show median of SFU/10^6 splenocytes per neoepitope.

volumes reached an average of 50 mm^3, the mice received i.m. 1×10^9 TU of LV::A7, LV::UBA7 or Ctrl LV (Fig. 4a, b). In contrast to LV::A7, LV::UBA7 induced a significant inhibition of tumor growth compared to Ctrl LV at day 30 (Fig. 4b). This trend was also observed at the suboptimal LV dose of 1×10^8 TU (Supplementary Fig. 3) without any transient phase of tumor eradication was observed with both LV::A7 and LV::UBA7. Ultimately, a treatment with LV::UBA7 only fully controlled MC38 WT growth in mice that had already completely eradicated the MC38 NeoAg tumor (Fig. 3). In this context, the host immune system not only developed vaccine-induced responses which controlled MC38 NeoAg growth, but was also exposed to the full antigenic repertoire of the MC38 tumor and certainly developed responses against other tumor antigens as well which allowed further eradication of the MC38 WT tumor.

To determine the relationship between the intensity/diversity of the T cell responses (Fig. 2) and the anti-tumor effect induced by LV::UBA7 and LV::A7, specific T cells were assessed in the spleen, tumor, tumor-draining lymph nodes (tdLNs) (Fig. 4c, d) or contralateral inguinal lymph nodes (Supplementary Fig. 4) on day 20, i.e., at the peak of the anti-tumor response. The T cell response was quantified by intracellular staining of IFNγ and TNFα in $CD4^+$ (Fig. 4c) or $CD8^+$ (Fig. 4d) T cells. Responses were detected only in the $CD8^+$ subset. Both LV::A7- and LV::UBA7-induced responses were detectable in the spleen, tdLNs and tumor, but not in the contralateral inguinal lymph nodes, indicating specific presence of the induced T cells in the secondary lymphoid organs able to insure tumor immune surveillance. No neoepitope-specific responses were detected in the Ctrl LV-treated tumor bearing mice, indicating that the tumor per se was not immunogenic, at least against the neoepitopes tested. The total responses detected in the spleen and tumor were significantly higher in LV::UBA7- than LV::A7-treated mice in contrast to the previous observations (Fig. 2). The key distinction between these two experiments lied in the immunization context; the former was conducted prophylactically in naïve mice, while the latter employed a therapeutic approach in tumor-bearing mice. We cannot rule out the possibility that exposure of the host immune system to the tumor may have an impact on the profile of neoantigen-specific T-cell responses. The higher potential of LV::UBA7 over LV::A7 induce a readily detectable T cell response against the sub-dominant Dpagt1 neoepitope was confirmed in both tdLNs suggesting its broader immunospecificity (Fig. 2 and Supplementary Fig. 4).

The intensity of the T cell response was correlated in the tumor, spleen, and tdLNs against the dominant Cpne1 and the subdominant Irgq neoepitopes. However, a higher response was noted against the dominant Adpgk neoepitope in the spleen, with minimal response in the tdLN. Conversely, for the sub-dominant Dpagt1 neoepitope, the response was much more intense in the tdLNs and inside the tumor compared to the spleen. To test whether the lack of intra-tumoral Adpgk-specific T cells could result from the loss of the corresponding allele in the treated mice, a previously published whole exome sequencing dataset from MC38 (Kerafast cell line) was used to estimate the variant allele frequency (VAF) and the representation of

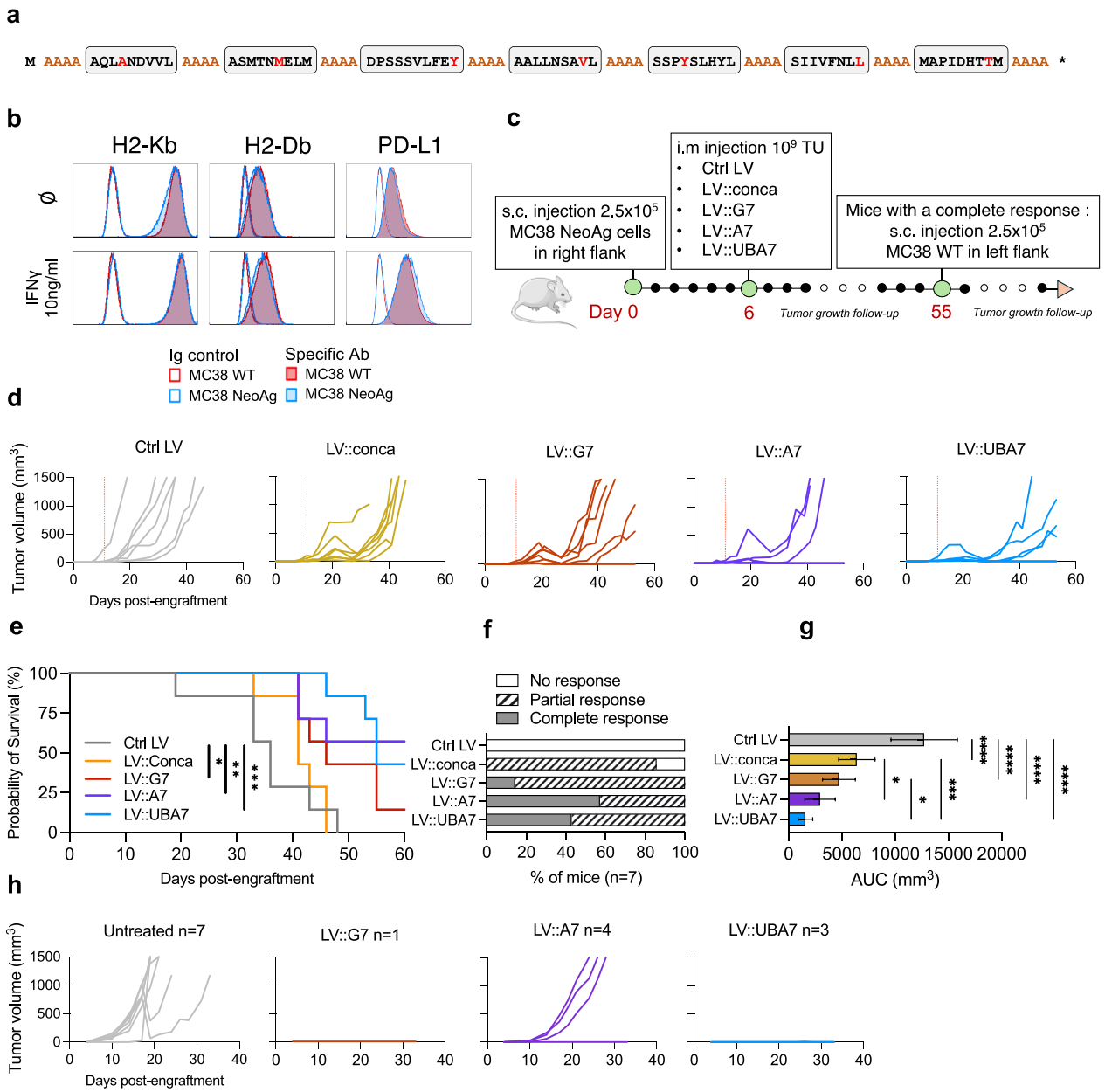

Fig. 3 | Anti-tumor therapeutic efficacy of LV-based vaccines encoding optimized poly-neoepitopes. a Amino acid sequence of the MC38 neoepitope fusion used to generate MC38 NeoAg cell line (**b**) Cytometric verification of the surface expression of H2-K^b, H2-D^b and PD-L1 by MC38 WT and MC38 NeoAg. **c** Experiment timeline. **d** Tumor growth follow-up in individual mice ($n = 7$). **e** Individual Kaplan–Meier survival curves. **f** Percentage of mice with no response (no tumor growth slowdown or regression on 2 consecutives measures), partial response (tumor growth slowdown or regression on 2 consecutives measures but detectable tumor), or complete response (tumor regression and undetectable tumors until day 55). **g** Mean AUC of tumor growth curves shown in **d** with standard deviations ($n = 7$). Statistical significance was determined by using one-way ANOVA (* = $p < 0.05$, *** = $p < 0.001$, **** = $p < 0.0001$). **h** Tumor growth follow-up after a rechallenge with 2.5×10^5 MC38 WT cells in the opposite flank in the cured mice.

the concerned mutations in the total tumor cell population[26]. This analysis validated the presence of Aatf, Cpne1, Dpagt1, Irgq, Med12, but not of Adpgk and Reps1 neomutations in the MC38 used in this study (Supplementary Table 1), thus correlating the absence of Adpgk mutation and that of intra-tumor Adpgk-specific T cells.

Inclusion of natural sequences flanking the minimal epitopes enhances the intensity and diversity of LV-induced T cell responses

To better reflect the reality of personalized neoantigen-based immunotherapy which requires identification of neo-mutations with high neoantigenic potential and insertion of the most relevant neoepitopes into the vaccine design, we used in a new series of LVs containing 27-mers peptides, centered around the selected neo-mutations instead of the minimal sequences. To this end, each epitope used in the non-optimized LV::conca and optimized LV::UBA7 were extended to their natural N- and C-terminal flanking regions to reach 27-mers centered on the neo-mutations (Fig. 5a). This approach enables a vaccine to include sequences encompassing all potential MHC-I (8- to 11-mer) and MHC-II (up to 14-mer) epitopes potentially generated by the neo-mutation and thus maximizes the probability of T-cell induction.

The immunogenicity of the resulted "LV::conca-27" and "LV::UBA7-27" vectors was assessed versus that of LV::conca and LV::UBA7 by IFNγ ELISPOT on splenocytes (Fig. 5b). LV::conca-27 induced a more diversified

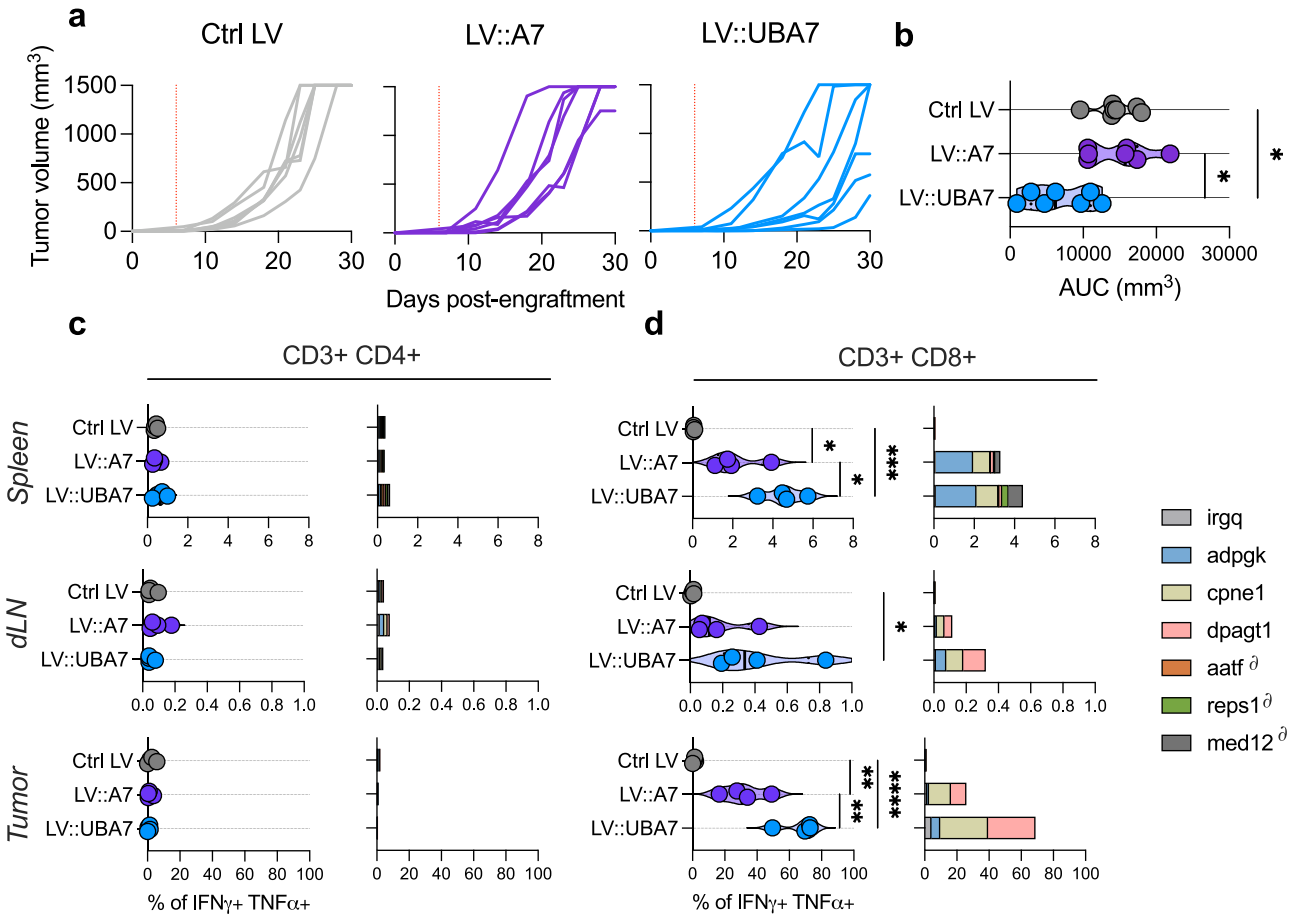

Fig. 4 | LV::UBA7 treatment delayed tumor growth via enhanced intra-tumoral T cell infiltration compared to LV::A7. Mice were engrafted s.c. with 2.5×10^5 MC38 WT at day 0 and were then treated i.m. with 1×10^9 TU of Ctrl LV, LV::A7 or LV::UBA7 at day 6 ($n = 7$). **a** Tumor growth curves. Red line indicates the day of vaccine treatment. **b** Area under curves (AUC) of tumor volume at the end of the experiment, i.e., day 30. **c**, **d** Mice were engrafted s.c. with 2.5×10^5 MC38 at day 0, followed by i.m. injection with 1×10^9 TU of Ctrl LV, LV::A7 or LV::UBA7 at day 6 ($n = 4$). On day 20, spleen, tumor and tdLNs were collected. Cells were incubated for 18 h with individual synthetic 9-to-11-mer peptides and the specific response was monitored by intracellular staining of IFNγ and TNFα in $CD3^+$ $CD4^+$ (**c**) or $CD3^+$ $CD8^+$ (**d**) T cells. The left panel shows the cumulative percentage of $IFN\gamma^+$ $TNF\alpha^+$ T cells for all neoepitopes in individual mice. The right panels present stacked bar graphs of the median of percentages of $IFN\gamma^+$ $TNF\alpha^+$ T cells for each neoepitope. "∂" indicates the peptides tested only in the spleen. Gating strategy is described in Supplementary Fig. 2. Statistical significance was determined using a one-way ANOVA (* = $p < 0.05$, ** = $p < 0.01$, *** = $p < 0.001$, *** = $p < 0.0001$).

response than LV::conca (Fig. 5c), yet with an equal total intensity (Fig. 5d). In contrast to LV::conca which polarized most of the response towards the Cpne1 neoepitope, LV::conca-27 induced a T cell response with a diversity of specificities close to that induced by LV::UBA7 or LV::UBA7-27 (Fig. 5e).

The immunogenicity of LV::UBA7 and LV::UBA7-27 was comparable in terms of diversity, with readily detectable responses against all neoepitopes in the majority of mice (Fig. 5e). However, significantly higher overall intensity was detected for LV::UBA7-27, even though the responses to Cpne1 or Reps1 neoepitopes tended to be lower (Fig. 5d). Therefore, the use of long sequences encompassing the minimal epitopes favored the intensity and diversity of neoepitope-specific T-cell immunity.

LV-based immunotherapy eliminates specifically the MC38 tumor cells bearing the targeted neo-mutations

To investigate the neo-mutation repertoire in the residual tumors of LV-treated mice, we used the VAF approach at the endpoint of the experiment (Fig. 6a–c). We preliminary validated the presence of neo-mutations in cultured MC38 WT cells and their absence in C57BL/6 healthy colon tissue (Fig. 6d). To estimate intratumor VAF changes, residual MC38 WT tumors were collected and the loci containing the relevant neo-mutations were amplified. PCR products were combined and sequenced by NGS. VAF changes were assessed by counting the reads featuring the neo-mutation or the wild-type allele. (Fig. 6e, f). We observed that the VAF values of MC38 WT tumors from the Ctrl LV group was close to those of cultured MC38 WT cells (Fig. 6d). In contrast, LV-based immunotherapy induced changes in MC38 WT VAF for certain neo-antigens in a manner dependent on both the mutation and the LV vector (Fig. 6e). Specifically, all LV reduced the Cpne1-associated VAF relative to the control, indicating that Cpne1 mutation-bearing cells were underrepresented within the tumor at the experiment endpoint. This reduction of Cpne1 VAF, also correlated with the stronger vaccine-induced anti-Cpne1 immunity in the spleen (Fig. 5), indicating a specific neo-mutation loss under a selective immune pressure. LV::conca treatment reduced VAF only for the Cpne1 neo-mutation, in correlation with the highly focused anti-Cpne1 response. In contrast, LV::UBA7-27 and, to a lesser extent, LV::UBA7, both reduced VAF across all other neo-mutations. LV::conca-27 treatment impacted VAF only for the Cpne1 and Irgq neo-mutations. Finally, we observed that the used MC38 WT line lacked the targeted Adpgk and Reps1 mutations, explaining the absence of TILs specific to these mutations (Fig. 4). Having seen no change in the VAF for the TP53 mutation (a generic tumor driver mutation used here as control), we get further convinced of the neo-antigen specificity of the established immune response.

Even if all tumors from treated individuals showed VAF reduction of targeted mutations, those mutation remained still detectable at the genome level.

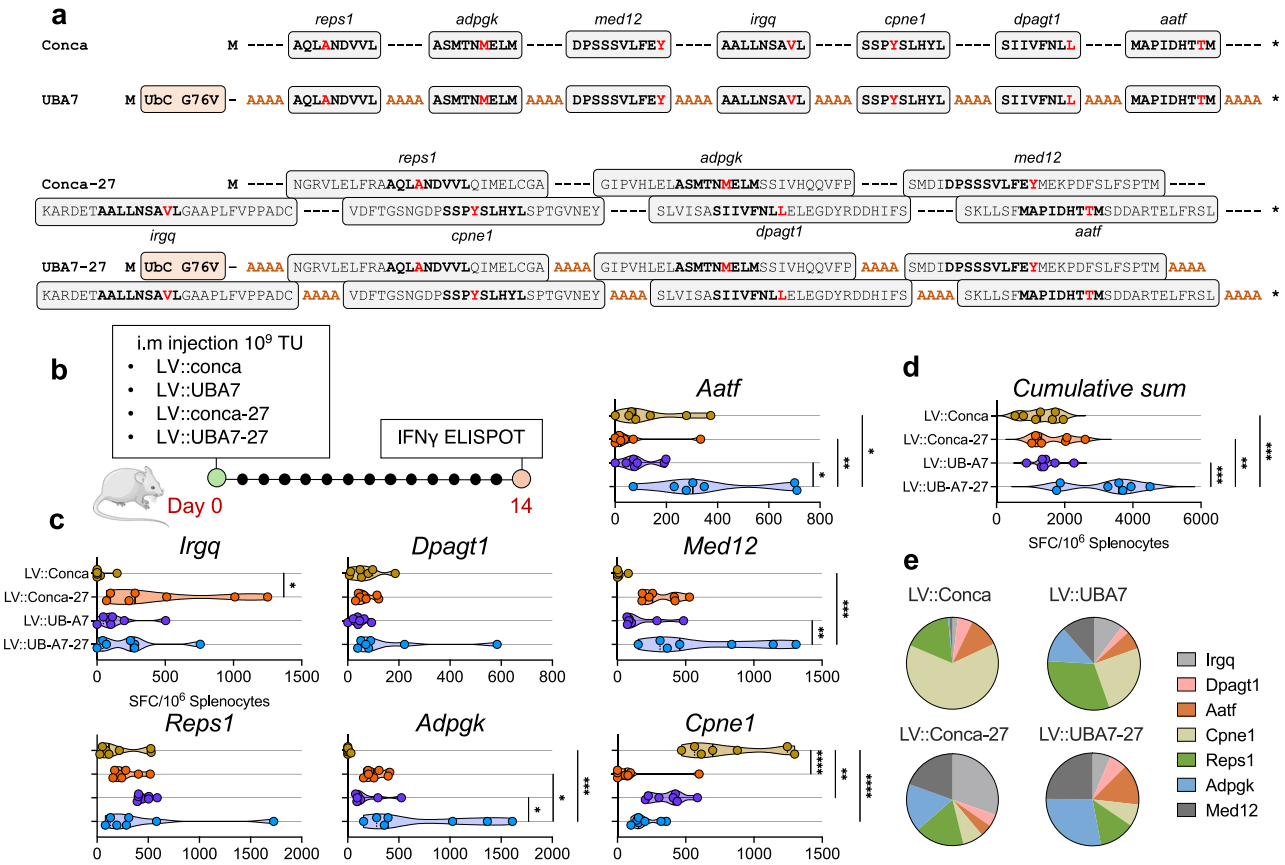

Fig. 5 | Impact on T-cell responses of poly-neoepitope design containing 27-mer sequences encompassing the neoepitopes versus minimal neoepitopes. a Amino acid sequences of MC38-specific poly-neoepitopes, without or with proteasome-addressing tag or 4-alanine spacers. Transgenes were introduced into LV previously described in Fig. 1. Boxes represent selected neoepitopes. Bold characters indicate the sequence of the synthetic peptide used in IFNγ ELISPOT (**c**). Mutated peptides are indicated in red. **b** Experiment timeline. Mice were immunized i.m. with 1×10^9 TU of individual LVs ($n = 7$). **c** Fourteen days later, IFNγ ELISPOT was applied to splenocytes stimulated with appropriate synthetic peptides. SFU per million splenocytes of individual mice against each peptide. **d** Cumulative sum of the measured response against all peptides for each individual mouse. **e** Diversity of the response (median) against all tested peptides per group. Statistical significance was determined using a one-way ANOVA. (* = $p < 0.05$, ** = $p < 0.01$, *** = $p < 0.001$).

The observed immune tumor escape unlikely to result from transcriptional changes of the targeted neoepitope, as determined by quantification of the neoantigen transcripts in RT-qPCR from the tumors at the endpoint (Fig. 6g)[27]. However, this assay is incapable of discriminating the mutant and the wild-type allele expression.

Anti-tumor benefit of combined LV::UBA7 and anti-PD1 immunotherapy

There are several lines of evidence that T cell responses to neoepitopes are not as strong as those specific to fully non-self, pathogen-derived antigens[28]. Unleashing the anti-neoepitope T cell immunity by anti-check point inhibitors has been previously showed to be beneficial[29]. MC38 WT cell line stably expresses surface PD-L1 which contributes to inhibit anti-tumor T cell cytotoxicity[30,31]. To evaluate a possible benefit of combined LV::UBA7 and anti-PD1 immunotherapy, 2.5×10^5 MC38 WT cells were s.c. inoculated into C57BL6/J mice. At day 6, when the average of tumor volume reached ≈50 mm^3, mice were treated i.m. with LV::UBA7-27 or Ctrl LV. From day 9, mice were injected intraperitoneally (i.p.), twice a week and during 3 weeks, with 200 µg of an antagonistic anti-PD1 monoclonal antibody (αPD1) or a control Ig isotype (Iso) (Fig. 7a). Although LV::UBA7-27 + Iso or Ctrl LV + αPD1 already combination induced significant tumor growth delay compared to Ctrl LV + Iso (Fig. 7b), survival extension was further extended in the LV::UBA7-27 + αPD1 group (Fig. 7c). Until cessation of the αPD1 treatment at day 30, whereas in the LV::UBA7-27 + αPD1 group the tumors grew little or not at all, continued growth was observed in the 3 other groups (Fig. 7d). However, no tumor elimination was observed in either group. Discontinuation of the αPD1 treatment drastically altered the immune balance, allowing the tumor to regain its immunosuppressive capacity, and continuous growth was observed in all groups.

Extension to an alternative neoantigen assortment

We generated a new set of LVs encoding an optimized polyantigen, composed of 9 CD4 and CD8 neoepitopes from CT26 colon carcinoma cell line, derived from the BALB/c (H-2^d) strain (Fig. 8a)[13,14]. The same optimization procedures were applied as for MC38 neoantigens. The immunogenicity of the vectors was assessed in BALB/c mice through IFNγ and TNFα intracellular staining in CD4 (Fig. 8c–e) and CD8 (Fig. 8f–h) T splenocytes. LV::UBA7-27-CT26, which has the proteasome addressing ubiquitin C tag and 4-alanine spacers between 27-mer consecutive antigenic fragments, induced the most intense (Fig. 8c, d) and the most diverse (Fig. 8e) $CD8^+$ T splenocyte responses. This result was consistent with the former observations in the MC38 model. In addition, a stronger $CD4^+$ T cell response was observed for LV::UBA7-27-CT26 compared to LV::conca-CT26 and LV::A7-CT26 (Fig. 8f, g) without difference in terms of diversity (Fig. 8h). This indicated that the backbone optimizations enhanced not only MHC-I- but also MHC-II-restricted antigen presentation. Interestingly, LV::conca-27-CT26 induced a higher cumulative response compared to LV::conca-CT26 (Fig. 8g). However, this increase was not due to a higher response against each peptide but rather to a near-exclusive focus on the Tmem87 neoepitope (Fig. 8f). This result suggests that the absence of a spacer

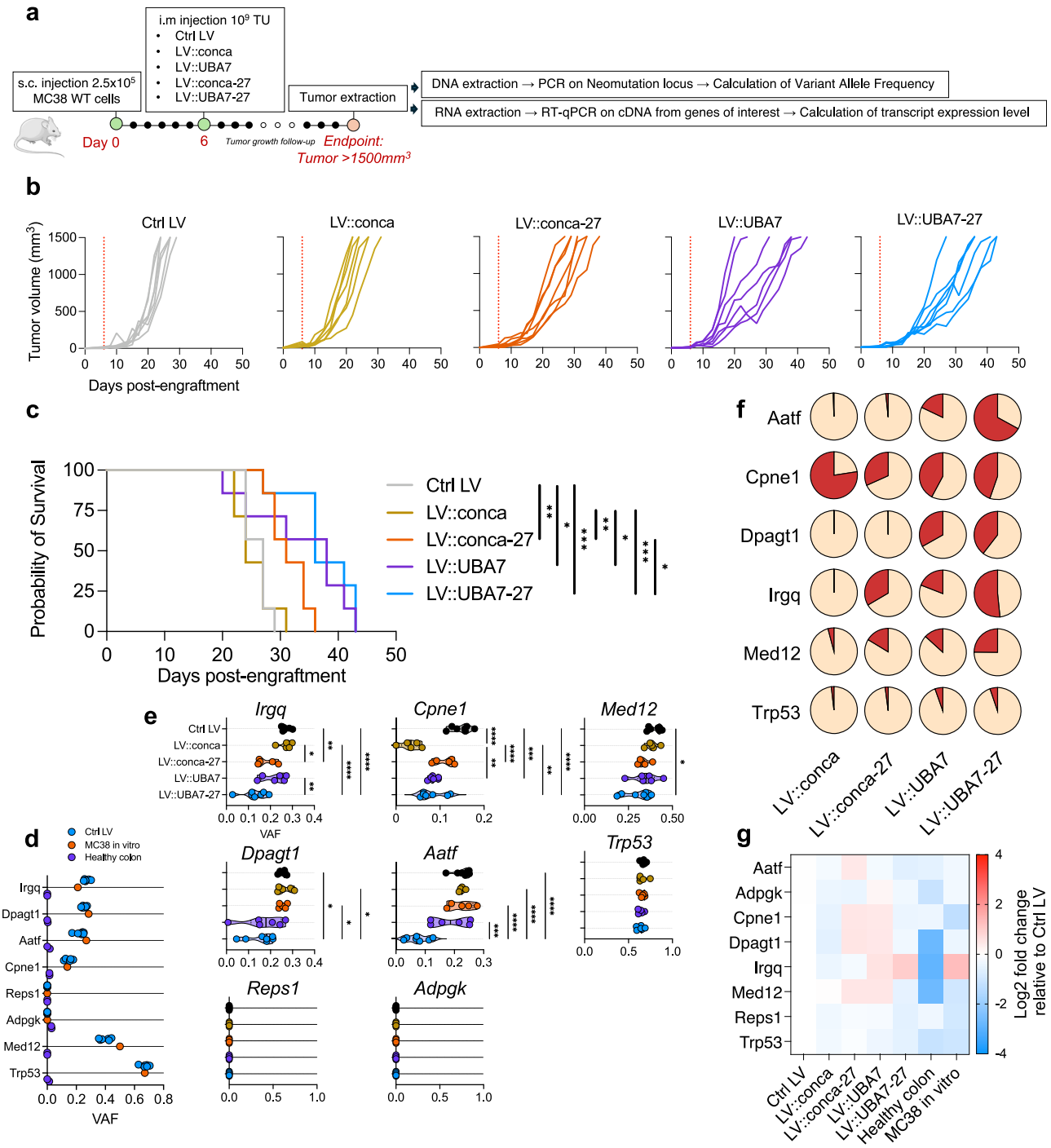

Fig. 6 | Therapeutic vaccination specifically eliminated MC38 WT tumor cells bearing the targeted neo-mutations. Mice were engrafted s.c. with 2.5×10^5 MC38 WT cells at day 0 and were then vaccinated on day 6 with 1×10^9 TU of various LV ($n = 7$). DNA and RNA were extracted from the tumors. Neo-mutation loci were amplified by PCR on genomic DNA, and VAF was analyzed by NGS (**d**–**f**). Transcript levels of mutated genes were quantified by RT-qPCR on RNA-derived cDNA (**g**). **a** Experiment timeline. **b** Tumor growth curves. **c** Kaplan–Meier survival analysis. **d** VAF comparison for neo-mutations in healthy colon tissue from female C57BL6/j mice ($n = 2$), cultured MC38 ($n = 1$), and MC38 tumors from the mice treated with Ctrl LV ($n = 7$). **e** VAF of neo-mutations in tumors treated with each of the LV vaccines. **f** Mean percentage loss of VAF (red) for each neo-mutation in tumors from vaccinal LV-treated mice relative to tumors from Ctrl LV-treated mice. **g** Heatmap of transcript expression changes for neo-mutated genes, normalized on β2m transcripts and compared to the Ctrl LV group. Statistical significance was determined by log-rank test for survival (**c**), and by one-way ANOVA for VAF comparisons (**e**). (* = $p < 0.05$, ** = $p < 0.01$, *** = $p < 0.001$, **** = $p < 0.0001$).

promotes a response against certain epitopes at the expense of others, both in a 27-mer context and in minimal epitope settings.

To assess the antitumor efficacy, BALB/c mice were engrafted s.c. with 2.5×10^5 CT26 cells and were treated i.m. at day 6 with 1×10^9 TU of LV vaccines (Fig. 8i). A significant tumor growth delay was observed on day 28 only in mice treated with LV::UBA7-CT26-27 compared to Ctrl LV (Fig. 8j). Collectively, these findings corroborated the previous results generated in the MC38 model regarding the optimization of the backbone. In fact, (i) proteasome-addressing tag, (ii) use of 4-alanine spacers, and (iii) incorporating long 27-mer sequences encompassing the relevant neoepitopes, contributed to improve the intensity/diversity/anti-tumor effect of the T cells induced by the LV vectors.

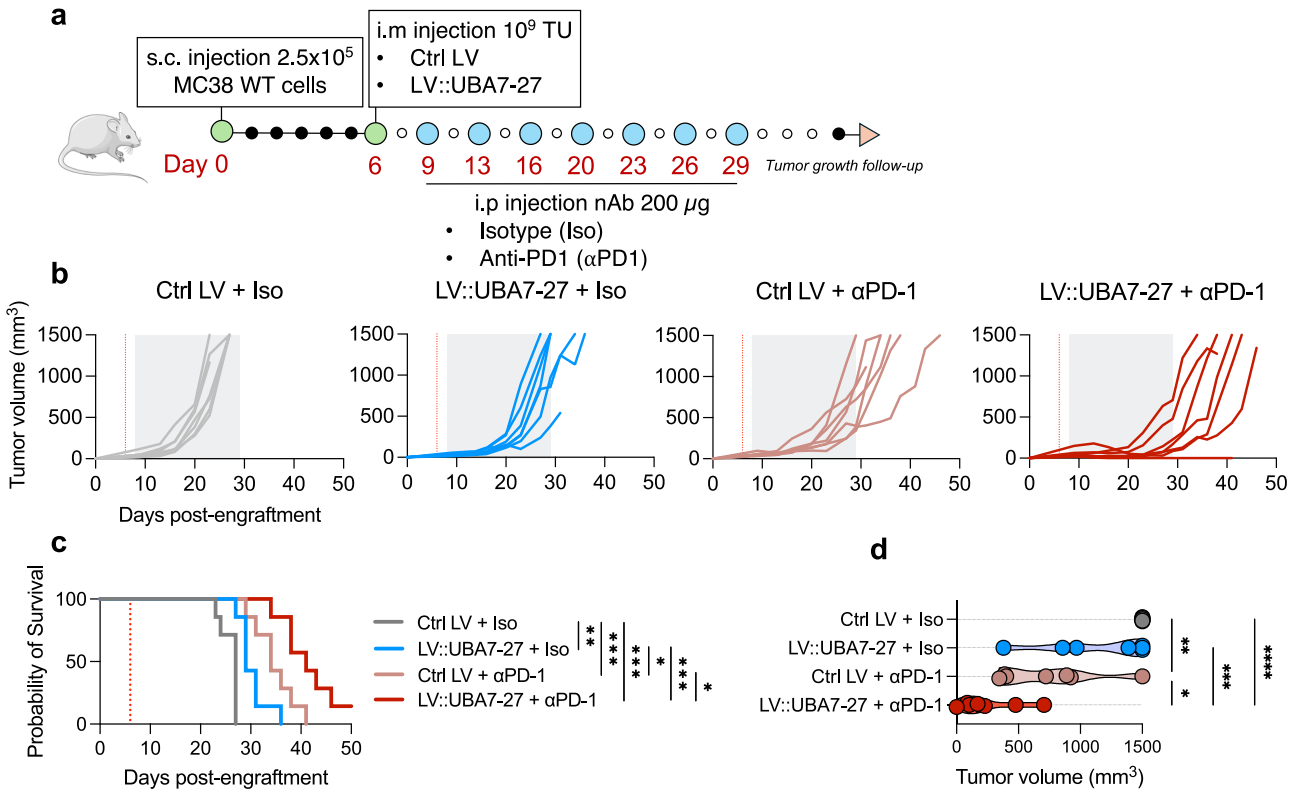

Fig. 7 | Improved anti-tumor effect of LV::UBA7-27 when combined to an antagonistic anti-PD1 treatment. C57BL6/J mice were injected s.c. with 2.5×10^5 MC38 WT at day 0 and were then injected i.m. with 1×10^9 TU per mouse of Ctrl LV or LV::UBA7-27 at day 6 ($n = 7$). Mice were injected i.p. with 200 μg of either αPD1 antibody or an isotype control (iso) at day 9 and then twice a week for 3 weeks. **a** Experiment timeline. **b** Tumor growth curves. Red line = the time point of LV injection. Gray area = antibody treatment interval. **c** Kaplan–Meier survival curves. **d** Tumor size at the end of αPD1 or iso treatment (day 29). Statistical significance was determined using a log-rank test (**c**) or a one-way ANOVA test (**d**). * = $p < 0.05$, ** = $p < 0.01$, *** = $p < 0.001$, **** = $p < 0.0001$).

Discussion

Poly-antigen cleavage is crucial for the proper antigen orientation to the presentation machinery, transport and trimming, which is essential for the efficient loading onto MHC I molecules. These properties must be considered for successful vaccine design. In this study, we demonstrated advantage of using an optimized poly-antigenic backbone for the robust and diverse T cell response against a set of tumor neoantigens to be used in immunotherapy. The optimization strategy combined the addition of a proteasome-targeting sequence at the N-terminus of the poly-neoantigen and the insertion of hydrophobic 4-alanine spacers between consecutive neoepitopes. The resulting LV constructs were tested across a panel of 7 or 9 neoepitopes derived respectively from two colorectal tumor models, MC38 and CT26[12–14].

To improve proteasome targeting, we added to our original poly-antigen the following moieties: (i) a monomer of ubiquitin C to the N-terminus (ii) the PEST sequence directly engaging the ubiquitination machinery, to the C-terminus.

LVs encoding either of these constructs demonstrated enhanced neoepitope immunogenicity compared to LV encoding the same neoepitopes without such optimization. Notably, the optimized antigen designs resulted into eliciting T cell responses against sub-dominant MC38 neoepitopes. This observation is in line with previous results with DNA-based vectors inducing T cell immunity against subdominant epitopes derived from various viral antigens or (neo)onco-antigens[32–35]. The sub-dominance of (neo)epitopes may result not only from their low affinity for the MHC molecule's presentation groove, but also and above all from their low probability of being generated by proteasomal cleavage[36].

Ubiquitinated proteins can be processed by both the 20S and 26S proteasome subunits, while non-ubiquitinated forms of the same proteins are predominantly associated with the 20S proteasome[37]. Peptide pools generated by these two proteasome subunits are sufficiently distinct to ensure the production of a diverse array of immunogenic epitopes[38]. Therefore, proteasome targeting potentiates the diversification of the epitope repertoire from the complex poly-neoantigen encoded by the LV vaccine design.

Spacers composed of hydrophobic residues, are preferentially recognized by the constitutive proteasome and immunoproteasomes to the detriment of charged residues at the initial position. This favors peptide presentation, as the affinity of most murine or human MHC-I molecules is high for peptides with hydrophobic C-termini[39]. In line with a previous study[33], we provided additional in vivo evidence that spacers composed of alanine enhanced T cell induction against the selected neoepitopes, outperforming an apolar spacer composed of glycine. Indeed, the use of highly hydrophobic spacers between consecutive neoepitopes can preserve the latter from the proteasomal cleavage which can otherwise abrogate T cell induction[36]. SLVR spacers known to improve cathepsin cleavage[25], did not improve $CD8^+$ T cell induction by LV, which generally induces endogenous antigen presentation. SLVR spacers exert their effect via cross-presentation involving the endosomal/lysosomal pathway involving cathepsin[25].

We showed that T-cell response polarization toward specific epitopes could occur in the case of adjacent epitopes without spacers. This cannot be explained by affinity competition, as the spacer-containing constructs consistently induced broader responses than the constructs containing strictly concatenated epitopes. The issue likely lies in antigen processing, where efficient presentation depends on precise cleavage between epitopes. Since proteasomal cleavage preferentially occurs at hydrophobic residues that are also anchor residues for murine MHC-I H2-K^b and H2-D^b [39,40], lack of a favorable inter-epitope cleavage site may lead to intra-epitope cleavage and epitope destruction. Consequently, high-affinity epitopes might not be presented if the cleavage context is

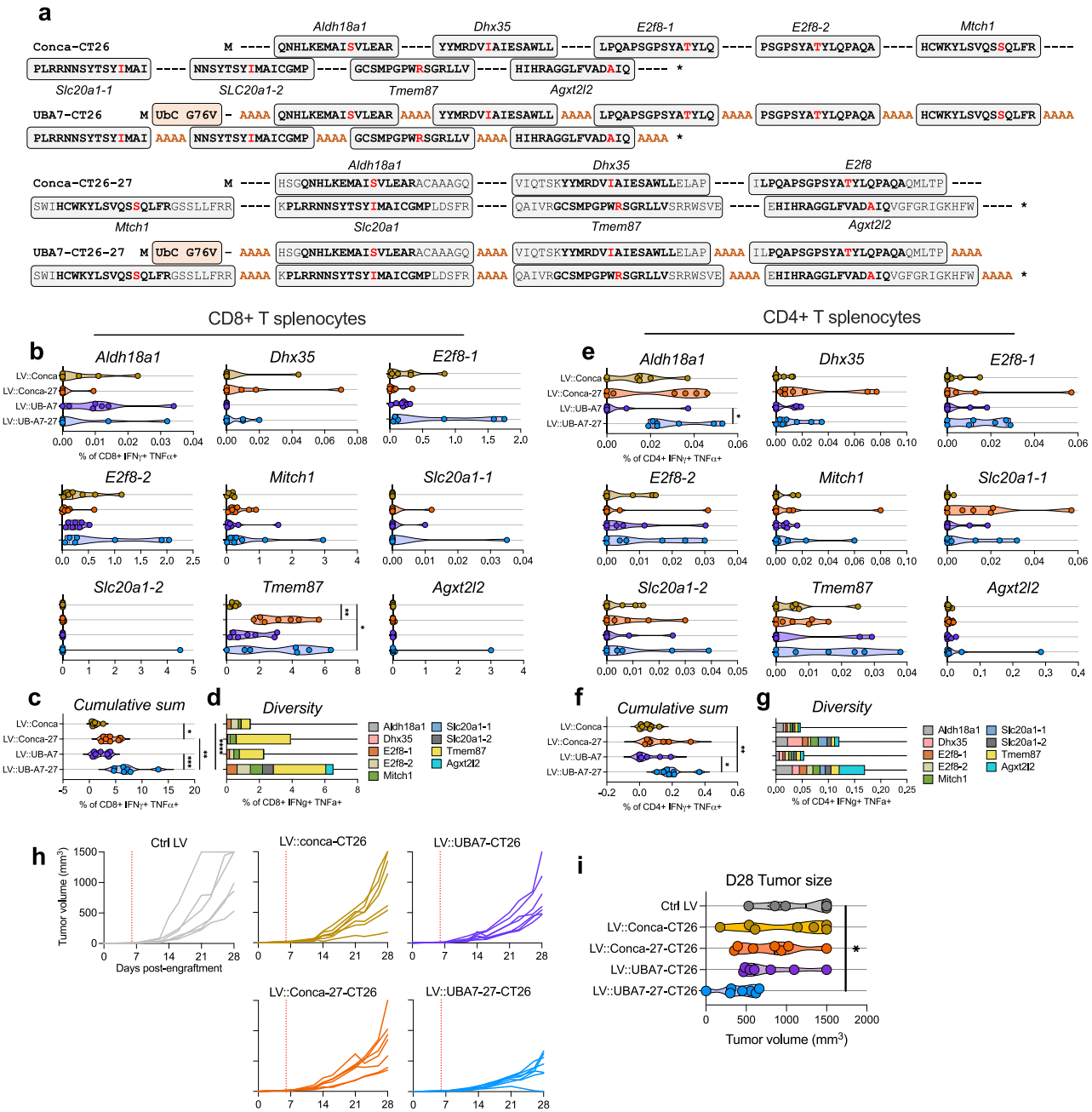

Fig. 8 | Backbone-optimized LV::UBA7-27-CT26 enhanced T cell response intensity, diversity, and anti-tumor effect in the CT26 tumor model. **a** Optimization of CT26-derived neoepitopes. Selected CD8$^+$ CT26-specific neoepitope sequences are indicated in white boxes, spacer sequences in brown, and proteasome addressing sequences in boxes. UbC G76V: Mouse ubiquitin C with the G76V mutation that prevents cleavage. PEST: PEST sequence from mouse Ornithine Decarboxylase. Transgenes were introduced into LV previously described in Fig. 1. Boxes represent selected neoepitope sequences from each Neo-Ag. Bold characters indicate the sequence of the 15-mer peptides used in in vitro T-cell assays (**b**, **c**). Mutated peptides are indicated in red. BALB/c mice were injected i.m. with 1×10^9 TU of each LVs ($n = 7$). Fourteen days later, spleens were collected and TNFα and IFNγ production by CD8$^+$ (**b**–**d**) or CD4$^+$ (**e**, **f**) T splenocytes were monitored after stimulation with appropriate peptides by flow cytometry. Percentage of CD8$^+$ (**b**) or CD4$^+$ (**e**) T cells producing both TNFα and IFNγ. **c**, **f** Cumulative sum of the measured response against all peptides for each individual mouse. **d**, **g** Diversity of the response (median) against all peptides tested per group. **h** BALB/c mice were injected s.c. with 2.5×10^5 CT26 at day 0 and were then injected i.m. with 1×10^9 TU per mouse of each LVs or Ctrl LV as control at day 6 and tumor growth was monitored ($n = 7$). Red line = the time point of LV injection. **i** Comparison of tumor size at the end point (day 28). Statistical significance was determined using a one-way ANOVA (**b**, **c**, **e**, **f**, **i**) (* = $p < 0.05$, ** = $p < 0.01$, *** = $p < 0.001$).

suboptimal[41]. This problem can also be translated to human epitopes and HLA anchor residues, such as the predominant HLA-A*02:01 allele for which the presence of a hydrophobic aa in position 2 of the epitope favors anchoring and presentation[40]. The lack of diversity in the T-cell response induced by concatenated constructs can be partially compensated by using 27-mer segments which introduce natural spacer regions allowing inter-epitope cleavage.

Notably, natural flanking sequences adjacent to the epitopes enhanced the intensity of the T cell response. This is in accordance with a previous study, which had shown that natural flanking residues can significantly influence the transporter associated with antigen processing (TAP)-dependent translocation of peptides with suboptimal transportability[42]. This observation supports the rationale for incorporating peptide sequences flanking the neo-mutations when designing poly-neoantigens. In addition,

for neoantigens with no prior experimental validation or precise epitope localization, this approach ensures comprehensive coverage of all potential MHC-I and -II neoepitopes.

The intensity of the immune response against neoantigens is obviously not the only determinant of an immunotherapy efficacy. Above all, the tumor's genetic mosaicism determines its sensitivity to immunotherapy. Indeed, the anti-tumor efficacy of LV::UBA7 therapy was much greater against the MC38 NeoAg tumors constitutively and homogeneously expressing the selected neoepitope set than against the parental MC38 tumors with mutanome heterogeneity, which favors their escape under the immune pressure. For instance, although the Cpne1 neo-mutation was one of the most immunogenic neoepitope, its low prevalence in the in vivo established MC38 tumors reduced the tumor sensitivity to the anti-tumor LV vaccines. This underscores the importance of designing antigenic constructs that incorporate the broadest possible diversity of neoepitopes to ensure maximum immune coverage in the context of tumor genetic mosaicism. Antigenic designs that capitalize on a wide antigenic repertoire can exert significant anti-tumor effect, shown here for LV::UBA7 and LV::UBA7-27 applied to MC38 and CT26 WT tumors. However, in these models no complete tumor regression was achieved with the vaccination alone.

In patients with untreated non-small cell lung cancer, neoantigen editing has been reported through local clearance of neoantigen-bearing tumor cells or subset-specific transcriptional downregulation[43]. Post-treatment sequencing of tumors in our study revealed a reduction in the VAF of the targeted neo-mutations, indicating a potential acceleration of immunoediting through vaccination. This was accompanied by a negative selection of cells lacking the targeted neo-mutation. No significant changes in the transcriptional levels of genes harboring these neo-mutations were observed. Transcriptional variations in neo-mutations linked to epigenetic regulation or reduction in the neo-mutation copy number, have been commonly reported in human cancers[43,44]. We cannot rule out that, in the fast-growing murine tumors studied here, the duration of our experiments was not sufficient for these mechanisms to become established and detectable.

One of the limitations of our study was the limited pool of neoantigens, which constrained the potential coverage of tumor heterogeneity and may have led to only partial tumor regression. Furthermore, two of the neo-mutations, previously described in the literature were not detected in the MC38 WT clone used in this study. In a murine tumor model, we were able to establish the proof of concept for the relevance of an optimized design to address the challenge of tumor heterogeneity. However, this model captures only one aspect of the complexity of real human tumors. Additional factors must be considered, such as structural barriers that limit immune cell access to the tumor, the presence of a suppressive tumor microenvironment that impairs immune activation, and secondary tumor sites that may exhibit genetic mosaicism distinct from the primary lesion[45]. To better address these issues, more complex and clinically relevant models could be employed in future studies. For instance, patient-derived xenograft (PDX) tumors implanted into mice with a humanized immune system may offer more informative insights.

Recent studies have shown that incorporating multiple copies of a given epitope into antigen-clustering designs enhanced its presentation by MHC-I molecules and specific T cell induction[46]. This approach, combined with the optimized backbone presented in this study, can further strengthen T cell response against dominant and sub-dominant neoepitopes. Given that the maximum transgene capacity of LVs is ≈5 kb without significantly affecting the vector production yield, an LV based on the LV::UBA7-27 design could potentially accommodate up to 50 neoantigens. However, there are also reports suggesting that the broader and more diverse the immunogens, the weaker the response against each individual epitope tends to be[47].

Neo-antigen-based vaccination may induce off-target responses if the neo-epitope-specific TCRs cross-react with the corresponding WT epitopes, as we observed here for Dpagt1, Aatf, Reps1, and Med12. Despite the ubiquitous expression of these proteins, implicated in metabolism (Dpagt1), signaling (Reps1), RNA synthesis (Med12), and transcriptional regulation (Aatf), throughout our experiments no macroscopic pathology was observed in mice vaccinated with LV vaccines targeting the MC38-derived neoepitopes. To date, no adverse events resulting from such off-target cross-reactive responses have been reported in the numerous clinical trials conducted in the field of neoantigen-based immuno-oncotherapy[48,49]. However, in humans, neoantigen selection must be approached with cautious, with careful assessment of expression levels and tissue distribution of the neoantigens to target. The patient life expectancy and risk-benefit ratio in advanced cancers must also be considered.

Integrating these elements into the balance between the intensity and diversity of the desired immune response, alongside factors such as the prevalence of neoantigen in tumors, the stability of their expression, the risk of T-cell cross-reactivity with WT sequences and the extraordinary polymorphism of HLA molecules, remains a major challenge in the design of clinically relevant neoantigen-based immunotherapies.

Material & methods

Lentiviral plasmid constructs and LV production

All genes underwent *Mus musculus* codon optimization and were synthetized by MWG Eurofins before being inserted into a pTRIP-β2m-Wm backbone via restriction digest and ligation between BamHI and XhoI sites[50]. The Ctrl LV features a non-coding adapter in place of the transgene. LV particles were generated through triple calcium phosphate transfection of HEK293T cells with (i) a plasmid (pTRIP) encoding the vector RNA carrying the gene of interest, (ii) a plasmid (pVSV-G) encoding the VSV-G Indiana envelope protein, and (iii) a plasmid (pNDK D64V) encoding packaging proteins comprising an integrase-defective pol protein resulting from the D64V substitution. At 48 h post-transfection, supernatants were harvested and clarified by centrifugation at 2500 rpm at 4 °C for 6 min. LVs were concentrated via ultracentrifugation at 82,700 *g* for 60 min. Pellets were resuspended in a buffer at pH 7.2 containing 20 mM PIPES (Sigma), 75 mM NaCl (Sigma), and 2,5% sucrose (Sigma), aliquoted, and stored at −80 °C. The LV titers, defined as TU per mL, was determined using a previously described method[51]. The titer represents the number of LV particles per mL capable of transferring viral genetic material into the reference HEK293T cells via transduction in the presence of 8 µM aphidicolin which blocks cell division.

Mice

Female C57BL/6JRj mice, aged between 6 to 8 weeks, were bought from Janvier (Le Genest Saint Isle, France). They were housed at the animal facilities of Institut Pasteur, Paris, France. The mice were subjected to standardized light–dark cycles and provided with ad libitum access to food and water. All experimental procedures involving mice were conducted in strict adherence to European and French regulatory guidelines (Directive 86/609/CEE and Decree 87-848 of 19 October 1987), following approval from the Institut Pasteur Safety, Animal Care and Use Committee, as well as the local ethics committee (CETEA #DAP190130), and sanctioned by the French Ministry of High Education and Research (APAFIS#16381-2018080217194542 v1, APAFIS# 20981-20190606164112731).

In vivo tumor models and treatments

MC38 (Kerafast, ENH204-FP) or CT26 (ATCC, CRL-2638) tumor cells were cultured following provider instructions. MC38 or CT26 tumor cells (2.5×10^5 mouse) were injected s.c. into the flank of C57BL/6 or BALB/c mice, respectively. To prevent movement and pain during the injection, mice were anesthetized by isoflurane exposure with a dose of 3% for induction and maintained at 1.5%. In a therapeutic vaccination setting, 6 days after the tumor engraftment, awake mice were randomized and injected i.m. with a single injection of LVs in 50 µl of PBS after manual restraint. If specified, aPD1 antibody (clone RMP1-14, BioXCell) or Ig control (clone 2A3, BioXCell) were given 3 days after immunization. Antibody was administered i.p. twice a week at a dose of 200 µg per mouse on awake animals after manual restraint. Monitoring of tumor growth was performed on awake mice after manual restraint 2 or 3 times a week with a

digital caliper. Tumor volume was estimated as a sphere using the V = L × W x W/2 formula, where V is the volume, L the length, and W the width. Mice were killed by cervical dislocation according to predefined endpoints, i.e., when tumor size reached 1500 mm^3 or started to become ulcerated, or when animals exhibited signs of cachexia, prolonged behavioral abnormalities, or physical impairment.

Immunization

For the immunogenicity assessments, C57BL/6 awake mice were immunized i.m. with 1×10^9 TU of LV in 50 µL after manual restraint.

IFNγ ELISPOT assay

As previously described[50], T splenocyte responses were evaluated using IFNγ ELISPOT assay after in vitro stimulation with peptide. Splenocytes from individual immunized mice were processed by homogenization, filtration through 70 µm-pore filters, and centrifugation at 450 g for 5 min. Cells were then treated with Red Blood Cell Lysing Buffer (Sigma), washed twice with PBS, and enumerated using a Chemometec (Nucleocounter NC-200) cell counter. Splenocytes were then seeded in flat-bottom 96 well plates at 1;× 10^5 cells per well in 200 µL of RPMI-GlutaMAX supplemented with 10% heat-inactivated fetal calf serum, 100 U/mL penicillin, 100 mg/mL streptomycin, 1×10^{-4} M non-essential amino acids, 1% vol/vol HEPES, 1×10^{-3} M sodium pyruvate, and 5×10^{-5} M of β-mercaptoethanol in ELISPOT plates (Millipore). The cells were either left unstimulated or were stimulated with appropriate peptide at a final concentration of 2 µg/mL or with 5 µg/mL of Concanavalin A (Sigma) as a functionality control. Each sample was conducted in triplicate, adhering to the manufacturer's guidelines. The plates were subsequently analyzed using an Immunospot CTL Immunospot S6 ultimate-V Analyzer (CTL).

Tumor-infiltrating cells and lymph node cells isolation

Tumor from individual mice were treated with Tumor Dissociation Kit (Miltenyi Biotech) and then homogenized by use of GentleMacs (Miltenyi Biotech) following manufacturer instructions. Cells were then filtered through 70 µm-pore filters (Miltenyi Biotech) and centrifuged at 400 *g* during 8 min. Cells were centrifuged for 20 min at 2100 *g* at RT without brake on gradient medium (Lympholyte M, Cedarlane Laboratories) and mononuclear cells were recovered.

Lymph nodes were harvested from killed mice and dissected under sterile conditions. Following exposure, lymph nodes were carefully excised and transferred to a dish containing complete RPMI medium. Gentle mechanical disruption and mincing of the tissue facilitated the release of lymph node cells into the medium. After centrifugation, the cell pellet was resuspended in an appropriate buffer for downstream applications. Cell count and viability assessment were performed, and the isolated cells were immediately used for experimental assays.

Intracellular cytokine staining

Splenocytes, mononuclear cells from tumors and isolated cells from lymph nodes were rinsed with PBS containing 1% bovine serum albumin (BSA) (FACS buffer), followed by a 25-min incubation at room temperature with a mixture of Near IR Live/Dead (Invitrogen), FcγII/III receptor blocking anti-CD16/CD32 (clone 2.4G2), PerCP-Cy5.5-anti-CD3ε (clone 145-2C11), EF450-anti-CD4 (clone RM4-5), and FITC-anti-CD8 (clone 53-6.7) monoclonal antibodies (BD Biosciences or eBioscience). Cells were subsequently washed twice in FACS buffer, permeabilized using the Cytofix/Cytoperm kit (BD Bioscience), and washed twice with PermWash 1X buffer from the Cytofix/Cytoperm kit before incubation with a mixture of PE-anti-TNF-α (clone MP6-XT22) and APC-anti-IFNγ (clone XMG1.2) antibodies for 30 min at 4 °C. Following incubation, cells were washed twice in PermWash and once in FACS buffer, then fixed for 5 min with Cytofix (BD Biosciences). Data acquisition was performed using an Attune NxT cytometer system (Invitrogen), and FlowJo software (Treestar, OR, USA) was used for data analysis.

Tumor extraction

Tumors were removed at the end point when the volume reached 1500 mm^3, minced into 2–3 mm^3 pieces, placed into lysing matrix D (MP Biomedical) containing appropriate lysis buffer for either RNA or DNA extraction and homogenized during 30 s at 6.0 m/s using MP Biomedical Fastprep 24 Tissue Homogenizer (MP Biomedical).

Targeted locus amplification and sequencing

Genomic DNA was extracted using Masterpure complete DNA & RNA Purification Kit (Lucigen) following manufacturer instructions. PCR on 9 neo-mutations loci were performed using HiFi cloneAmp PCR premix and purified by gel extraction using Gel and PCR Clean-up (Macherey-Nagel). The primers used are listed in the Supplementary Table 2. PCR products (around 85 bp) for 8 neoantigens were combined for each sample. These mixtures were A-tailed and indexed by ligation of Truseq DNA indexes (Illumina). Electrophoretic profiles showed a minor peak of 220 bp corresponding to indexed fragments. To enrich the libraries for the target 220-bp specie, the products of ligation reaction were pooled, purified on twice using AMPure XP magnetic beads (Beckman-Coulter; sample/beads ratio 1/1.2). and verified by electrophoresis on an 5300 Fragment Analyzer system (Agilent). Pools were sequenced on an Illumina Miseq system (Illumina) in a 2 × 150 bp dual-indexed mode. Loading concentration was 5 pM. 12% PhiX control was added to compensate for the library's low diversity. Each sample received from 3000 to 7500 150-bp reads.

Variant allele frequency calculation

Paired-end Fastq files were aligned against the reference *Mus musculus* genome (GRCm38 - mm10) using BWA-MEM software[52], filtering/removing duplicate using Samtools[53], variant calling using DeepVariant[54], normalized using Bcftools[53] annotated and analyzed using Snpeff/SnpSift[55]. Workflow was performed using Galaxy platform[56]. VAF was calculated as follows: AD (Variant) / (AD (Reference) + AD (Variant)) where AD refers to Allele Depth.

Quantification of antigens transcripts by qRT-PCR

Total RNA was extracted by using RNeasy Protect Mini Kit (Qiagen) according to the manufacturer's procedure. cDNA generation and RT-PCR reaction were described elsewhere[57]. The β2-microglobulin gene was used as an endogenous reference control to normalize differences in the amount of input nucleic acid. Difference of expression level was determined by using the comparative ΔΔCT method[27]. The fold change in gene expression was further calculated using $2^{-\Delta\Delta CT}$. The primers used are listed in the Supplementary Table 3.

Statistical analyses

Prior to One-way ANOVA test, normal distribution of each group was tested using a Shapiro-Wilk test ($p < 0.05$). Statistical analysis was performed using Prism GraphPad v9.

Data availability

The published article includes all datasets generated and analyzed during this study. All plasmids and lentiviral vectors generated in this study will be available under an MTA for research use. Further information and requests for resources and reagents should be directed to and will be fulfilled by the corresponding author francois.anna@pasteur.fr. NGS sequencing datasets generated during the current study are available in the Biostudies online repository under accession number: S-BSST2013.

Received: 21 February 2025; Accepted: 15 June 2025;
Published online: 04 July 2025

References

1. Fan, T. et al. Therapeutic cancer vaccines: advancements, challenges and prospects. *Signal Transduct. Target. Ther.* **8**, 1–23 (2023).

2. Alexandrov, L. B. et al. Signatures of mutational processes in human cancer. *Nature* **500**, 415–421 (2013).
3. Jia, Q. et al. Local mutational diversity drives intratumoral immune heterogeneity in non-small cell lung cancer. *Nat. Commun.* **9**, 1–10 (2018).
4. Martínez-Jiménez, F. et al. Pan-cancer whole-genome comparison of primary and metastatic solid tumours. *Nature* **618**, 333–341 (2023).
5. Peng, M. et al. Neoantigen vaccine: an emerging tumor immunotherapy. *Mol. Cancer* **18**, 1–14 (2019).
6. Ku, M. W. et al. Lentiviral vector induces high-quality memory T cells via dendritic cells transduction. *Commun. Biol.* **4**, 1–16 (2021).
7. Cousin, C. et al. Persistence of integrase-deficient lentiviral vectors correlates with the induction of STING-Independent CD8+ T Cell Responses. *Cell Rep.* **26**, 1242–1257.e7 (2019).
8. Luis, A. The old and the new: prospects for non-integrating lentiviral vector technology. *Viruses* **12**, 1103 (2020).
9. Ku, M. W., Charneau, P. & Majlessi, L. Use of lentiviral vectors in vaccination. *Expert Rev. Vaccines* **20**, 1571–1586 (2021).
10. Somaiah, N. et al. First-in-class, first-in-human study evaluating LV305, a dendritic-cell tropic lentiviral vector, in sarcoma and other solid tumors expressing NY-ESO-1. *Clin. Cancer Res.* **25**, 5808–5817 (2019).
11. Pollack, S. M. et al. First-in-human treatment with a dendritic cell-targeting lentiviral vector-expressing NY-ESO-1, LV305, induces deep, durable response in refractory metastatic synovial sarcoma patient. *J. Immunother.* **40**, 302–306 (2017).
12. Yadav, M. et al. Predicting immunogenic tumour mutations by combining mass spectrometry and exome sequencing. *Nature* **515**, 572–576 (2014).
13. Salvatori, E. et al. Neoantigen cancer vaccine augments anti-CTLA-4 efficacy. *npj Vaccines* **7**, 1–10 (2022).
14. Viborg, N. et al. DNA based neoepitope vaccination induces tumor control in syngeneic mouse models. *NPJ Vaccines* **8**, 77 (2023).
15. Kim, P. K., Hailey, D. W., Mullen, R. T. & Lippincott-Schwartz, J. Ubiquitin signals autophagic degradation of cytosolic proteins and peroxisomes. *Proc. Natl. Acad. Sci. USA* **105**, 20567–20574 (2008).
16. Komander, D. & Rape, M. The ubiquitin code. *Annu. Rev. Biochem.* **81**, 203–229 (2012).
17. Andersson, H. A. & Barry, M. A. Maximizing antigen targeting to the proteasome for gene-based vaccines. *Mol. Ther.* **10**, 432–446 (2004).
18. Ye, M., Morello, C. S. & Spector, D. H. Strong CD8 T-Cell responses following coimmunization with plasmids expressing the dominant pp89 and subdominant M84 antigens of murine cytomegalovirus correlate with long-term protection against subsequent viral challenge. *J. Virol.* **76**, 2100–2112 (2002).
19. Leachman, S. A. et al. Ubiquitin-fused and/or multiple early genes from cottontail rabbit papillomavirus as DNA vaccines. *J. Virol.* **76**, 7616–7624 (2002).
20. Loetscher, P., Pratt, G. & Rechsteiner, M. The C terminus of mouse ornithine decarboxylase confers rapid degradation on dihydrofolate reductase. Support for the pest hypothesis. *J. Biol. Chem.* **266**, 11213–11220 (1991).
21. Rechsteiner, M. & Rogers, S. W. PEST sequences and regulation by proteolysis. *Trends Biochem. Sci.* **21**, 267–271 (1996).
22. Xing, H., Hong, Y. & Sarge, K. D. PEST sequences mediate heat shock factor 2 turnover by interacting with the Cul3 subunit of the Cul3-RING ubiquitin ligase. *Cell Stress Chaperones* **15**, 301–308 (2010).
23. Zufferey, R., Donello, J. E., Trono, D. & Hope, T. J. Woodchuck hepatitis virus posttranscriptional regulatory element enhances expression of transgenes delivered by retroviral vectors. *J. Virol.* **73**, 2886 (1999).
24. Ferrington, D. A. & Gregerson, D. S. Immunoproteasomes: structure, function, and antigen presentation. *Prog. Mol. Biol. Transl. Sci.* **109**, 75 (2012).
25. Lynn, G. M. et al. Peptide–TLR-7/8a conjugate vaccines chemically programmed for nanoparticle self-assembly enhance CD8 T-cell immunity to tumor antigens. *Nat. Biotechnol.* **38**, 320–332 (2020).
26. Schrörs, B. et al. MC38 colorectal tumor cell lines from two different sources display substantial differences in transcriptome, mutanome and neoantigen expression. *Front. Immunol.* **14**, 1102282 (2023).
27. Livak, K. J. & Schmittgen, T. D. Analysis of relative gene expression data using real-time quantitative PCR and the $2^{-\Delta\Delta CT}$ method. *Methods* **25**, 402–408 (2001).
28. Custodio, J. M. et al. Structural and physical features that distinguish tumor-controlling from inactive cancer neoepitopes. *Proc. Natl. Acad. Sci. USA* **120**, e2312057120 (2023).
29. Carreno, B. M. et al. Cancer immunotherapy. A dendritic cell vaccine increases the breadth and diversity of melanoma neoantigen-specific T cells. *Science* **348**, 803–808 (2015).
30. Juneja, V. R. et al. PD-L1 on tumor cells is sufficient for immune evasion in immunogenic tumors and inhibits CD8 T cell cytotoxicity. *J. Exp. Med.* **214**, 895 (2017).
31. Hsu, J. et al. Contribution of NK cells to immunotherapy mediated by PD-1/PD-L1 blockade. *J. Clin. Investig.* **128**, 4654 (2018).
32. Velders, M. P. et al. Defined flanking spacers and enhanced proteolysis is essential for eradication of established tumors by an epitope string DNA Vaccine. *J. Immunol.* **166**, 5366–5373 (2001).
33. Aguilar-Gurrieri, C. et al. Alanine-based spacers promote an efficient antigen processing and presentation in neoantigen polypeptide vaccines. *Cancer Immunol., Immunother.* **72**, 2113–2125 (2023).
34. Li, L. et al. Optimized polyepitope neoantigen DNA vaccines elicit neoantigen-specific immune responses in preclinical models and in clinical translation. *Genome Med.* **13**, 1–13 (2021).
35. Duperret, E. K. et al. A synthetic DNA, multi-neoantigen vaccine drives predominately MHC Class I CD8+ T-cell responses, impacting tumor challenge. *Cancer Immunol. Res.* **7**, 174–182 (2019).
36. Niedermann, G. et al. Contribution of proteasome-mediated proteolysis to the hierarchy of epitopes presented by major histocompatibility complex class I molecules. *Immunity* **2**, 289–299 (1995).
37. Sahu, I. et al. The 20S as a stand-alone proteasome in cells can degrade the ubiquitin tag. *Nat. Commun.* **12**, 6173 (2021).
38. Emmerich, N. P. N. et al. The Human 26 S and 20 S proteasomes generate overlapping but different sets of peptide fragments from a model protein substrate. *J. Biol. Chem.* **275**, 21140–21148 (2000).
39. Winter, M. B. et al. Immunoproteasome functions explained by divergence in cleavage specificity and regulation. *Elife* **6**, e27364 (2017).
40. Reynisson, B., Alvarez, B., Paul, S., Peters, B. & Nielsen, M. NetMHCpan-4.1 and NetMHCIIpan-4.0: improved predictions of MHC antigen presentation by concurrent motif deconvolution and integration of MS MHC eluted ligand data. *Nucleic Acids Res.* **48**, W449–W454 (2020).
41. Gileadi, U. et al. Generation of an Immunodominant CTL Epitope Is Affected by Proteasome Subunit Composition and Stability of the Antigenic Protein. *J. Immunol.* **163**, 6045–6052 (1999).
42. Neisig, A. et al. Major differences in transporter associated with antigen presentation (TAP)-dependent translocation of MHC class I-presentable peptides and the effect of flanking sequences. *J. Immunol.* **154**, 1273–1279 (1995).
43. Rosenthal, R. et al. Neoantigen directed immune escape in lung cancer evolution. *Nature* **567**, 479 (2019).
44. Xie, N. et al. Neoantigens: promising targets for cancer therapy. *Signal Transduct. Target. Ther.* **8**, 1–38 (2023).
45. Goloudina, A., Le Chevalier, F., Authié, P., Charneau, P. & Majlessi, L. Shared neoantigens for cancer immunotherapy. *Mol. Ther. Oncol.* **33**, 200978 (2025).
46. Rappaport, A. R. et al. A shared neoantigen vaccine combined with immune checkpoint blockade for advanced metastatic solid tumors: phase 1 trial interim results. *Nat. Med.* **30**, 1013–1022 (2024).
47. Anna, F. et al. A lentiviral vector expressing a dendritic cell-targeting multimer induces mucosal anti-mycobacterial CD4+ T-cell immunity. *Mucosal Immunol.* **15**, 1389–1404 (2022).

48. Linette, G. P. & Carreno, B. M. Neoantigen vaccines pass the immunogenicity test. *Trends Mol. Med.* **23**, 869–871 (2017).
49. Lybaert, L. et al. Neoantigen-directed therapeutics in the clinic: where are we?. *Trends Cancer* **9**, 503–519 (2023).
50. Douguet, L. et al. Full eradication of pre-clinical human papilloma virus-induced tumors by a lentiviral vaccine. *EMBO Mol. Med.* **15**, e17723 (2023).
51. Iglesias, M. C. et al. A single immunization with a minute dose of a lentiviral vector-based vaccine is highly effective at eliciting protective humoral immunity against West Nile virus. *J. Gene Med.* **8**, 265–274 (2006).
52. Li, H. & Durbin, R. Fast and accurate long-read alignment with Burrows-Wheeler transform. *Bioinformatics* **26**, 589–595 (2010).
53. Danecek, P. et al. Twelve years of SAMtools and BCFtools. *Gigascience* **10**, giab008 (2021).
54. Poplin, R. et al. A universal SNP and small-indel variant caller using deep neural networks. *Nat. Biotechnol.* **36**, 983–987 (2018).
55. Cingolani, P. et al. A program for annotating and predicting the effects of single nucleotide polymorphisms, SnpEff. *Fly* **6**, 80–92 (2012).
56. Afgan, E. et al. The Galaxy platform for accessible, reproducible and collaborative biomedical analyses: 2018 update. *Nucleic Acids Res.* **46**, W537–W544 (2018).
57. Ku, M. W. et al. Intranasal vaccination with a lentiviral vector protects against SARS-CoV-2 in preclinical animal models. *Cell Host Microbe* **29**, 236–249.e6 (2021).

Acknowledgements

This work was funded by TheraVectys and Institut Pasteur. Yakov Vitrenko is supported by PAUSE programme, France Génomique (ANR-10-INBS-09) and IBISA. Mouse image used in Figs. 2, 3–8 is adapted from Servier Medical Art by Servier (https://smart.servier.com/), licensed under CC BY 4.0 (https://creativecommons.org/licenses/by/4.0/).

Author contributions

P.C. and F.A. conceptualized and designed experiments, I.F., B.V., P.A. and S.C. acquired data, F.A., A.N. and C.B. constructed and produced lentiviral vectors, I.F., B.V., L.M. and F.A. analyzed and interpreted the data, Y.V. performed deep sequencing, P.C. provided funding, L.M. and F.A. wrote the manuscript. All authors red and approved the final version of the manuscript.

Competing interests

P.C. is the founder and CSO of TheraVectys. B.V., I.F., A.N., P.A. and F.A. are employees of TheraVectys. LM has a consultancy activity for TheraVectys. Other authors declare no competing interests.

Additional information

Supplementary information The online version contains supplementary material available at https://doi.org/10.1038/s41541-025-01199-6.

Correspondence and requests for materials should be addressed to François Anna.